Modeling of a DC-RF Plasmathruster with the Navier-Stokes Code SINA

IEPC-2013-324

Presented at the 33rd International Electric Propulsion Conference,
The George Washington University • Washington, D.C. • USA
October 6 – 10, 2013

U. Bauder[1] and G. Herdrich[2] and S. Fasoulas[3]
Institute of Space Systems (IRS), University of Stuttgart, 70569 Stuttgart, Germany

and

M. Auweter-Kurtz[4]
German Aerospace Academy ASA, 71304 Böblingen, Germany

High power electric propulsion systems are currently under investigation with respect to planned and foreseen piloted exploration missions such as the human flight to Mars. For the further development and optimization of such electric thrusters numerical simulations can make a valuable contribution. The numerical models used for the simulations have to account for all important thermophysical aspects of the flow field within the thrusters. In order to simulate DC-RF plasma thrusters, not only the thermal and chemical non-equilibrium plasma flow has to be modeled, but also the DC and RF discharge. This paper describes the models that are implemented in the loosely coupled Navier-Stokes code SINA, which is being developed at the Institute of Space Systems (IRS). Preliminary results of a numerical simulation of the hybrid DC-RF thruster TIHTUS are presented and discussed.

Nomenclature

$\vec{A}^c$	=	complex vector potential
$\vec{B}$	=	magnetic flux density
β	=	Hall term
C	=	constant parameter in the Arrhenius equation
c_e	=	effective exit velocity
c_i	=	concentration of the species i
$D_{e,i}$	=	effective diffusion coefficient of species i
E	=	energy
$\vec{E}$	=	electric field
e	=	elementary charge
$\vec{F}$	=	vector of fluxes
H	=	enthalpy
$\vec{j}$	=	current density
K_c	=	equilibrium constant

[1] Scientist, Space Transportation Technology, bauder@irs.uni-stuttgart.de.
[2] Scientist, Head of Group Electric Propulsion and Plasma Wind Tunnels, herdrich@irs.uni-stuttgart.de.
[3] Professor, Head of Department Space Transportation Technology, fasoulas@irs.uni-stuttgart.de.
[4] Professor, Head of German Aerospace Academy, m.auweter-kurtz@german-asa.de.

k	=	Boltzmann constant
k_f, k_b	=	forward/backward reaction rate coefficient
λ	=	heat conductivity
M_{eff}	=	molecular mass of a mixture
n	=	iteration step
n_{mol}	=	number of molecular species
n_s	=	number of species
n_e	=	number density of electrons
$\nu'_{i,j}, \nu''_{i,j}$	=	stoichiometric coefficient for the species i in equation j
μ	=	viscosity
μ_0	=	permeability of free space
$\vec{\Omega}$	=	vector of sources
ω_i	=	rate of production of the species i
p	=	pressure
ψ_i	=	molar fraction of the species i
Ψ	=	current fundtion
$\vec{Q}$	=	vector of solutions
Q	=	exchange term for energy balance equations
q_r	=	source term of radiation transport
ρ	=	density
σ	=	electric conductivity
T	=	temperature
T_A	=	effective activation energy
T_e	=	electron temperature
T_{vib}	=	vibrational temperature
t	=	time
u, v, w	=	components of the velocity vector
$\vec{v}$	=	velocity
x, y, z	=	Cartesian coordinates

I. Introduction

High power electric propulsion systems are currently under investigation with respect to planned and foreseen piloted exploration missions such as the human flight to Mars. Besides magnetoplasmadynamic thrusters (both self-field and applied field MPD), high power arc-jets and high power ion thrusters, new concepts - in particular hybrid thruster systems - are in the scientific focus to meet the mission requirements by increased system flexibility in terms of specific impulse, thrust density and propellant requirements. The novel two-stage hybrid plasma thruster TIHTUS (Thermal-Inductively Heated Thruster of the University of Stuttgart) was developed and experimentally investigated at the IRS within the last years [1] on basis of the gathered expertise at the Institute of Space Systems (IRS) [2]. The device consists of two plasma sources put in series. The first stage is a $100\,\mathrm{kW}$water-cooled thermal arc-jet and the second stage consists of an inductively heated plasma source, as shown in Figure 1. Several measurement campaigns were undertaken during that time to proof the feasibility of the hybrid concept. The experiments show that the efficiency of the second stage is increased if it is used simultaneously with the first stage and that the overall thrust level is increased as well. The thrust level is around $2\,\mathrm{N}$ for an input power of $25\,\mathrm{kW}$ in each stage. Future projects at IRS aimed at increasing the input power level will increase the thrust level significantly. Within these projects, numerical simulations are planned in parallel with experimental measurement campaigns.

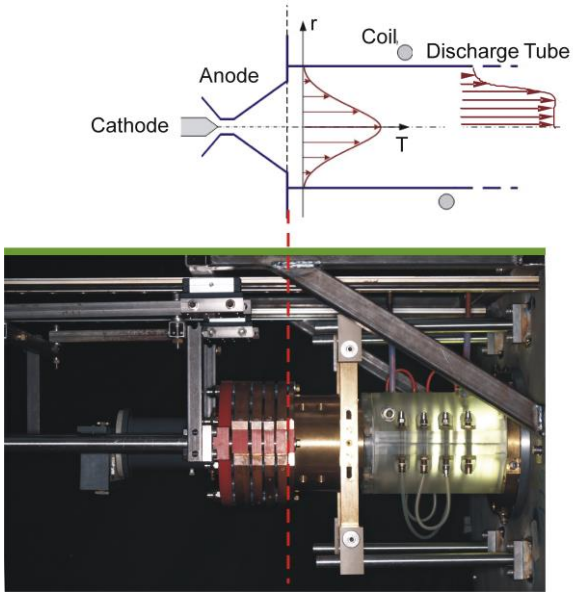

Figure 1 Sketch and photograph of TIHTUS [1]

The effective exit velocity of an electric propulsion system c_e is proportional to $\sqrt{T_0/M_{eff}}$. To increase the exit velocity, hydrogen or other lightweight gases are used as propellant for many electric propulsion systems, because of their low molecular mass M_{eff}. Typically, the pressure in such a device is low, the temperatures and velocities are high. The high temperatures of the gas lead to dissociation and ionization. Due to the low pressure, the collision frequencies are low and as a result the chemical and thermal relaxation times are also high. In combination with the high gas velocity, this causes chemical and thermal non-equilibrium within the physical domain of the thruster. Hence, in order to accurately simulate the plasma flow in an electric propulsion system, the physical model of the simulation must account for a non-equilibrium composition and multiple temperatures. This includes the model for the chemical composition as well as the model for the transport coefficients and the balance equations for the electron energy and the vibrational energies of the molecules. Additionally, the electromagnetic fields of the DC and/or RF discharge have to be taken into account and included in the model, i.e. the Maxwell equations have to be solved.

II. The Program System SINA

For the numerical simulation of thermal arc-jets and inductively coupled plasma sources the loosely coupled Navier-Stokes code SINA [1],[4] (Sequential Iterative Non-equilibrium Algorithm) is developed and used at the Institute of Space Systems (IRS). The iteration scheme of SINA is shown in Figure 2. In general, the equations that describe the non-equilibrium plasma flow with discharges can be solved fully coupled or loosely coupled. SINA uses a loosely coupled scheme and therefore, the main part of SINA consists of three solvers:

• The first solver within this loop computes the flow field with the assumption of a frozen flow. This so called NSF-solver (Navier-Stokes solver) accounts for total mass, total momentum and total energy conservation according to the Navier-Stokes equations.

• The second solver contains the equations that are necessary to describe the real gas effects: the chemical reactions, the equations for vibrational energy of the molecules and an electron energy balance equation. Within this so called CVE-solver, the conserved quantities of the solution from the first solver are kept constant.

• The third solver, which is the last within one total iteration loop, solves the discharge equation of an electric arc or an inductive discharge and provides the source terms for the total energy conservation equation and the momentum conservation equations of the first solver as well as the electron energy balance equation of the second solver for the next total iteration loop.

The total iteration loop is repeated until convergence is reached in all solvers and the result is the solution of the steady-state problem. Additionally, trajectories of dust particles within the flow as well as radiation transport can be accounted for using the particle solver [5] or the external program HERTA [6],[7] and the European radiation database PARADE [8] for the simulation of radiation transport phenomena. Since the coupling to the flow field solution is not as strong as for the chemistry and the electric discharge, these solvers are coupled to the iteration

scheme outside of the total iteration loop and are run only once per several total iterations for a numerical solution of a given steady-state problem.

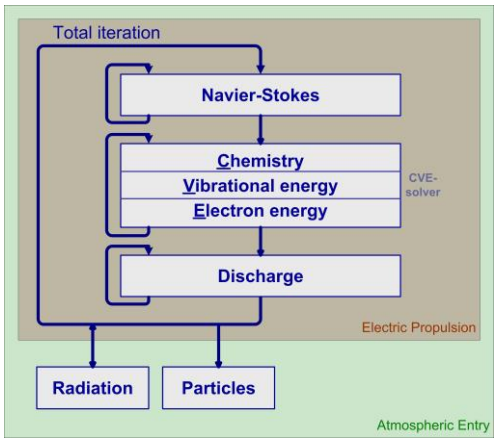

Figure 2 Iteration scheme of the loosely coupled method as it is used in SINA

The program system uses structured multiblock grids [9] to accurately discretize complex geometries. They are generated with GridPro [10]. On shared memory systems the grid blocks can be calculated in parallel using an OpenMP enabled version of the SINA.

III. Physical and Numerical Models

In this section, the physical and chemical models for the numerical simulation of a stationary viscous plasma flow in thermal and chemical non-equilibrium with electric DC and/or RF discharges are presented. First, the basic equations for the non-equilibrium plasma flow are given. They are implemented in the NSF and CVE solver of SINA. Second, the discharge equations are presented.

A. The plasma flow in thermal and chemical non-equilibrium

As already mentioned, the flow solver (NSF-solver) addresses the Navier-Stokes equations, i.e. the solver accounts for the conservation of the total mass, the total momentum and the total energy of the flow. The conservation of mass

$$\frac{\partial}{\partial t}\rho = -\nabla \rho \vec{v} \tag{1}$$

states, that the change of mass in time within a control volume is only possible by transportation of mass over the volume faces. This means that no mass can be created within the control volume. (An exception in this regard is the sublimation or evaporation of particles or droplets when the particle solver is used. Since multiphase flows are not covered in this paper, the source terms are neglected in Equation (1))

The second part of the Navier-Stokes equations are the momentum conservation equations that are given below for all three dimensions x, y and z:

$$\begin{aligned}\frac{\partial}{\partial t}\rho u = &-\nabla \rho u \vec{v} - \frac{\partial p}{\partial x} \\ &+ \frac{\partial}{\partial x}\left[2\mu\left(\frac{\partial u}{\partial x} - \frac{\nabla \vec{v}}{3}\right)\right] + \frac{\partial}{\partial y}\left[\mu\left(\frac{\partial u}{\partial y} + \frac{\partial v}{\partial x}\right)\right] \\ &+ \frac{\partial}{\partial z}\left[\mu\left(\frac{\partial u}{\partial z} + \frac{\partial w}{\partial x}\right)\right] + j_y B_z - j_z B_y,\end{aligned} \tag{2}$$

$$\begin{aligned}\frac{\partial}{\partial t}\rho v &= -\nabla \rho v \vec{v} - \frac{\partial p}{\partial y} \\ &+ \frac{\partial}{\partial x}\left[\mu\left(\frac{\partial v}{\partial x} + \frac{\partial u}{\partial y}\right)\right] + \frac{\partial}{\partial y}\left[2\mu\left(\frac{\partial v}{\partial y} - \frac{\nabla \vec{v}}{3}\right)\right] \\ &+ \frac{\partial}{\partial z}\left[\mu\left(\frac{\partial v}{\partial z} + \frac{\partial w}{\partial y}\right)\right] + j_z B_x - j_x B_z\end{aligned} \quad (3)$$

and

$$\begin{aligned}\frac{\partial}{\partial t}\rho w &= -\nabla \rho w \vec{v} - \frac{\partial p}{\partial z} \\ &+ \frac{\partial}{\partial x}\left[\mu\left(\frac{\partial w}{\partial x} + \frac{\partial u}{\partial z}\right)\right] + \frac{\partial}{\partial y}\left[\mu\left(\frac{\partial w}{\partial y} + \frac{\partial v}{\partial z}\right)\right] \\ &+ \frac{\partial}{\partial z}\left[2\mu\left(\frac{\partial w}{\partial z} - \frac{\nabla \vec{v}}{3}\right)\right] + j_x B_y - j_y B_x.\end{aligned} \quad (4)$$

In all three equations, on the left hand side we see the change of momentum in time and the first term on the right hand sides represents the change by convective transport over the control volumes faces. The second term on the right hand side describes the effects of pressure force, while the third term represents the viscous forces within the gas. Contrary to the mass conservation equation, there are source terms in the momentum conservation equation. These last two terms describe the source terms of the Lorentz force, which are a result of the discharge equation solved by the third solver of SINA. Again, forces generated by solid particles are neglected as well as gravitational effects.

The last part of the Navier-Stokes equation is the conservation equation for the total energy, which is in our case

$$\begin{aligned}\frac{\partial}{\partial t}E &= -\nabla H \vec{v} + \nabla \lambda \nabla T + \sum_{r=1}^{n_{mol}} \nabla \lambda_{v,r} \nabla T_{v,r} \\ &+ \nabla \lambda_e \nabla T_e - \frac{2}{3}\mu\left(\frac{\partial u}{\partial x} + \frac{\partial v}{\partial y} + \frac{\partial w}{\partial z}\right)^2 \\ &+ \mu\left[2\left(\frac{\partial u}{\partial x}\right)^2 + 2\left(\frac{\partial v}{\partial y}\right)^2 + 2\left(\frac{\partial w}{\partial z}\right)^2\right] \\ &+ \mu\left[\left(\frac{\partial u}{\partial y} + \frac{\partial v}{\partial x}\right)^2 + \left(\frac{\partial u}{\partial z} + \frac{\partial w}{\partial x}\right)^2 + \left(\frac{\partial v}{\partial z} + \frac{\partial w}{\partial y}\right)^2\right] \\ &+ \sum_{i=1}^{n_s} \rho_i H_i D_{e,i} \nabla \psi_i + \frac{\vec{j}^2}{\sigma} + \vec{v}\left(\vec{j} \times \vec{B}\right) - q_r.\end{aligned} \quad (5)$$

Again, the left hand side represents the temporal change of the volume specific total energy. The first terms on the right hand side describe the convective transport of enthalpy, the heat conduction of translational energy and the heat conduction of vibrational energy and of electron energy, respectively. The next two lines represent the transport of energy by viscous dissipation. In the last line, the first term describes the diffusion of the single components of the gas that also causes an energy transport. The next two terms are the source terms computed by the discharge solver, namely the ohmic heating and the energy caused by the Lorentz force. The very last term is the source term for energy gains or losses by radiation processes. These two source terms are very important for the coupling of the electric discharge or radiation to the flow field of SINA.

The inviscid fluxes are calculated using either the AUSM$^+$ [10] or AUSM$^+$-up [12] scheme with second order MUSCL-type reconstruction and various TVD-limiters [13]. A central difference scheme is used for the calculation of the viscous fluxes. The models for the transport properties of the plasma have to take into account the thermochemical non-equilibrium. In SINA they are computed using the models of Chapman and Cowling or Yos [14],[15]. The model of Chapman and Cowling generates more accurate results than the mixture rule of Yos when compared to experimental values in equilibrium. [20] The time integration within the flow field solver is done by an explicit 4-step Runge-Kutta scheme of 1st order in time [16].

The result of the subiteration of the Navier-Stokes solver can be regarded as a frozen flow. The CVE solver then computes the thermochemical composition of that flow regarding the non-equilibrium effects due to the high plasma velocity. The chemical composition is determined by solving the set of balance equations

$$\frac{\partial}{\partial t} c_i = -\nabla c_i \vec{v} + \omega_i + \rho D_{e,i} \nabla \psi_i \tag{6}$$

for the molar concentration c_i of each heavy species. Here, the first term on the right hand side is the convective transport, followed by the rate of production ω_i and the term for the mass diffusion of the components. The rate of production is given by

$$\begin{aligned} \omega_i = & \sum_{j=1}^{m} \left(\nu_{ij}'' - \nu_{ij}'\right) \\ & \left[k_{fj(T,T_e,T_{vib})} \prod_k c_k^{\nu_{kj}'} - k_{bj(T,T_e,T_{vib})} \prod_l c_l^{\nu_{lj}''} \right], \end{aligned} \tag{7}$$

where the summation is done over all m reactions. The stoichiometric coefficients are ν_{ij}' for the forward reaction j of the species i and ν_{ij}'' for the backward reaction. Accordingly, the rate coefficients are k_{fj} for the forward reaction j and k_{bj} for the backward reaction. They are computed employing the rate constants and the equilibrium constants of Park. The mole fraction of the electrons is computed with the assumption of quasineutrality in the plasma.

The second part of the CVE solver accounts for the vibrational temperatures of the uncharged molecules. This is done by solving the balance equations for the vibrational energy

$$\begin{aligned} \frac{\partial}{\partial t} E_{v,r} = & -\nabla E_{v,r} \vec{v} + \nabla \lambda_{v,r} \nabla T_{v,r} + \rho E_{v,r} D_{e,r} \nabla \psi_r \\ & + Q_{C-V,r} + Q_{T-V,r} + Q_{v,r-v,s} + Q_{e-V,r} \end{aligned} \tag{8}$$

For each neutral molecule r. The change of vibrational energy in time is caused by convective transportation, vibrational heat conduction, diffusion, energy gains or losses due to chemical reactions, coupling between vibrational and translational energy, relaxation processes between the vibrating molecules and by the coupling between vibrational and electron energy. Assuming a truncated harmonic oscillator model, the resulting vibrational energy leads to the vibrational temperatures.

The last part of the CVE solver is responsible for the solution of the electron energy balance equation

$$\begin{aligned} \frac{\partial}{\partial t} E_e = & -\nabla H_e \vec{v} + \nabla \lambda_e \nabla T_e + \rho H_e D_{e,m} \nabla \psi_e \\ & - Q_{C-e} - Q_{e-V} + Q_{T-e} - q_r + \frac{j^2}{\sigma} \end{aligned} \tag{9}$$

of the free electrons. On the left hand side we see the temporal change of electron energy. On the right hand side, this equation accounts for the convective transport, the heat conduction of the electrons, the diffusion and the energy gained or lost during ionization reactions. The fourth term represents the coupling of electrons and vibrating molecules as already seen in the vibrational energy conservation equation. After that, the coupling with the heavy particles' translational energy follows. The last two terms are the source terms for radiation and ohmic heating by an electric discharge, respectively. The electron temperature is derived from the electron energy according to

$$E_e = \frac{3}{2} n_e k T_e. \tag{10}$$

When all source terms on the right hand sides of Eqs. (6), (8) and (9) are combined to a vector $\vec{\Omega}$ and all fluxes are combined to $\vec{F}$, one can rewrite the main equations of the CVE solver to

$$\frac{\partial}{\partial t}\vec{Q} = -\nabla\vec{F} + \vec{\Omega} \tag{11}$$

where the solution variables are combined to a vector $\vec{Q}$. For the numerical model, the right hand side of Eq. (11) can be written as $\dot{\vec{Q}}$. This rate of change is zero when the steady state solution is reached. Therefore, one can implement a Newton scheme

$$\vec{Q}^{n+1} = \vec{Q}^{n} - \frac{\vec{Q}^{n}}{\partial\dot{\vec{Q}}^{n}/\partial\vec{Q}} \tag{12}$$

that determines a new $\vec{Q}^{n+1}$ so that the residual $\dot{\vec{Q}}$ tends to zero. The drawback of this implicit method is that we need the derivatives of $\dot{\vec{Q}}$. These derivatives for the Jacobian matrix can be computed analytically or by numerical derivation. In SINA, the rates and the exchange terms are derived analytically and only the fluxes numerically. The implicit Newton method itself is not stable for the stiff chemistry problems. Therefore, we add the inverse of an Euler time step to the main diagonal of the equation system and end up with the so called Newton time step method.

For the computation of the chemical composition, a detailed reaction scheme is needed. Since many plasma thrusters work with hydrogen as propellant, a reaction scheme for hydrogen is described here, but reaction schemes for other gases are implemented as well. (For re-entry simulations in the earth atmosphere, the 11 component model of Park [17] is used and for an entry simulation at mars, a 5 component model is implemented [5]. Their implementation is straightforward.) The reaction scheme of Scott [18] is often used for the simulation of hydrogen plasma thrusters [1],[2]. Some assumptions in this model do not fit to the physical models implemented in SINA, so changes are necessary. The model of Scott does not contain forward and backward reaction rates for each reaction, but only forward rates. If the model contains also a backward reaction, it is explicitly given as an additional forward reaction. In SINA, the forward reaction rate coefficient

$$k_f = CT^s e^{\frac{-T_A}{T}} \tag{13}$$

is defined by the Arrhenius equation where $T_A = E_A/R$ represents the effective activation energy as a temperature. The backward rate coefficient

$$k_b = \frac{k_f}{K_c} \tag{14}$$

is computed using the equilibrium constant K_c that is computed using the minimization of Gibbs free energy. This method has the advantage that the computed equilibrium is directly defined by the equilibrium constant instead of the fraction of k_f and k_b, but the method fails for artificial or composed forward reaction rate coefficients. Therefore, Scott's model has to be slightly changed. SINA takes into account backward reactions for all defined equations and all backward reaction rate coefficients are computed using the equilibrium constant.

Further changes to the reaction scheme of Scott are necessary due to the following assumptions and physical models in SINA. Currently, the implemented model for the vibrational energy is capable of 2-atomic molecules only. Linear 3-atomic molecules may be described approximately by a 2-atomic model, but this is not a legitimate option for the triangular shape of the H_3^+ ion. Therefore the 7-component model of Scott is reduced to a 6-component model neglecting H_3^+ and, of course, neglecting all equations involving that species. Due to the very low concentrations of H_3^+ this species has a minor influence on the resulting composition.

The excited states of the single species are not considered in the physical model of SINA, therefore all equations of Scott's model forming or removing excited species are omitted. Additionally, the chemical solver is not capable of radiation transport within the solver so the deionization of H^+ resulting in H and radiation is also neglected. In summary, this leads to the modified reaction scheme shown in [20]. For each of the 12 reactions, the backward reaction is always computed using the equilibrium constants. The considered species in these reactions are the 6 components: H, H_2, H_2^+, H^+, H^- and e^-.

The reaction schemes are provided as an input data file to SINA. For chemical equilibrium, the results compare well with the data from Patch [19]. While the dissociation of the hydrogen molecule is perfectly reproduced, there are slight discrepancies in the temperature range above the ionization [20].

The transport coefficients are computed by the models of Chapman and Cowling or Yos, as already mentioned. In both models, the transport coefficients are derived from rigorous gas kinetics and require the binary collision integrals as defined by Hirschfelder [21]. They are provided through polynomial coefficients in an input file. The viscosity, the effective diffusion coefficients, the electrical conductivity and the heat conductivity coefficients for translational, rotational vibrational and electron temperature are then computed according to the chemical non-equilibrium composition. Further details of the models can be found in the paper of Fertig [14] and results for hydrogen in [20].

B. The DC and RF discharge

In order to simulate thermal arcjets and inductively coupled plasma generators or the hybrid DC-RF thruster TIHTUS, a discharge solver is needed that is capable of both DC and RF discharges. An arbitrary electromagnetic field in space and time is in general described by the Maxwell's equations. For the DC and the RF discharge, different assumptions and simplifications can be made. Hence, at least in a first step, two separate solvers are used for the DC and RF discharge. For the DC discharge, Maxwell's equations and Ohm's law for plasma

$$\vec{j} = \sigma(\vec{E} + \vec{v} \times \vec{B}) - \frac{\omega_e \tau_e}{B}(\vec{j} \times \vec{B}) + \frac{\sigma}{e n_e} \nabla p_e \qquad (15)$$

are combined to the discharge equation [22]

$$\begin{aligned} &\frac{1}{\mu_0} \nabla \times (\frac{1}{\sigma} \nabla \times \vec{B}) - \nabla \times (\vec{v} \times \vec{B}) \\ &+ \frac{1}{\mu_0} \nabla \times (\beta(\nabla \times \vec{B}) \times \vec{B}) = 0. \end{aligned} \qquad (16)$$

The RF discharge is slightly more difficult to handle. Of course, Maxwell's equations are used again together with the reduced version

$$\vec{j} = \sigma(\vec{E} + \vec{v} \times \vec{B}) \qquad (17)$$

of Ohm's Law. Using the vector potential formulation $\vec{A^c}(t) = A^c e^{i\omega t}$ and $\vec{B(t)} = \nabla \times \vec{A^c}(t)$ as well as the Lorentz calibration, one can derive the discharge equation [23],[24]

$$\nabla^2 \vec{A^c} - i\omega\mu_0\sigma\vec{A^c} + \mu_0\sigma\vec{v} \times \nabla \times \vec{A^c} + \frac{\omega^2}{c^2}\vec{A^c} = 0 \qquad (18)$$

for a harmonic RF field within an ICP. Note, that the time dependency of the vector potential is cancelled out. This is not possible when Ohm's law in the extended formulation of equation (15) including the hall term $\vec{j} \times \vec{B}$ is used [25].

Both, the DC and the RF discharge equation are discretized with second order finite differences for the rotational symmetric case on the nodes of the two-dimensional structured multiblock grid. They are solved with a successive over-relaxation method (SOR) that is based on the Gauss algorithm. This rather simple algorithm is sufficient in terms of accuracy and computing costs. Since the solution of the DC and RF discharge equations is very fast compared to the solution of the equation systems in both the NSF and CVE solver, there will be only a small benefit in computing time with a faster converging algorithm for the discharge solver. The finite volume source terms for the NSF and CVE solver are taken as the arithmetic mean of the four grid nodes that define the 2D grid cell.

IV. Simulation and Results for the hybrid DC-RF thruster TIHTUS

At the institute of space systems (IRS), a hybrid thruster TIHTUS (Thermal-Inductively Heated Thruster of the University of Stuttgart) is being developed [1], which consists of a thermal arcjet as a first stage and an inductively heated plasma generator as a second stage. A sketch of the thruster is shown in Figure 3. The second stage is intended to afterheat the plasma plume of the first stage. The plume of the first stage is fast and hot in the center and relatively cold and slow in the outer region. The energy coupling of the ICP occurs near the wall in the cold region due to the skin effect. Thus, the plasma velocity will be increased by the power that is coupled into the flow by the ICP.

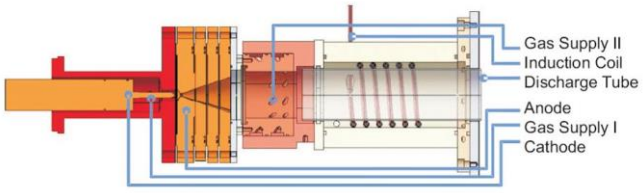

Figure 3. Drawing of the two stage hybrid thruster TIHTUS [1].
First stage (Arcjet) on the left side, second stage (ICP) at the right side and the injection head (Gas Supply II) in the middle.

The computational multiblock grid for the simulation consists of 36 structured grid blocks with 4894 cells in total and is shown in Figure 4. A mesh refinement at the solid wall boundaries increases the accuracy of the flow solution at the boundary layer. The boundary types are set directly in GridPro and translated into the proprietary format for SINA by a new transformation interface routine in the preprocessing step.

The injection boundary condition at the inflow iterates the pressure to maintain the mass flow rate of $\dot{m} = 300\,\mathrm{mg/s}$. The cathode wall is modeled with a non-slip boundary condition where the temperature is set to fixed temperatures between $2200\,\mathrm{K}$ at the base and $2900\,\mathrm{K}$ at the cathode tip according to experimental data from comparable thrusters. All other solid wall boundaries are set to a fixed wall temperature of $T_w = 500\,\mathrm{K}$. The outflow into the vacuum chamber is modeled with a pressure boundary condition with the experimentally measured value of $p_{exit} = 40\,\mathrm{Pa}$ is applied.

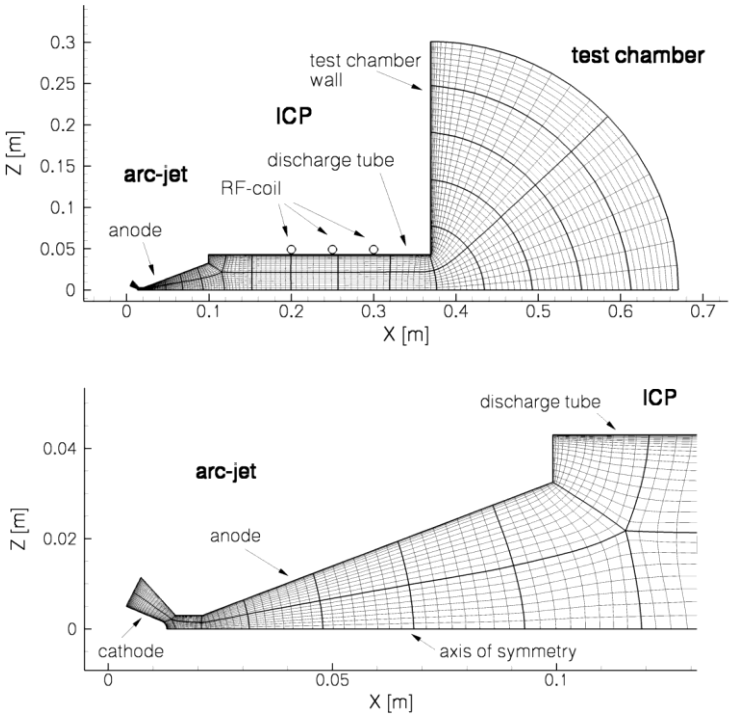

Figure 4 Structured multiblock grid with 36 grid blocks and 4894 cells in total
Complete grid (top) and enlarged view of the arc-jet stage (bottom)

The measured DC current of $I_{DC} = 238\,\mathrm{A}$ is applied to cathode and anode indirectly by the distribution of the current function Ψ along the electrodes. Thermionic emission at the cathode and the fluxes of the charged particles at both electrodes determine the current density distribution. The coil current for the RF discharge is set to $\hat{I}_{RF} = 96,5\,\mathrm{A}$ corresponding to the measured value in the experiment. The electric conductivity has to be limited by $\sigma > 80\,\mathrm{S/m}$ due to strong oscillations of the plasma flow when

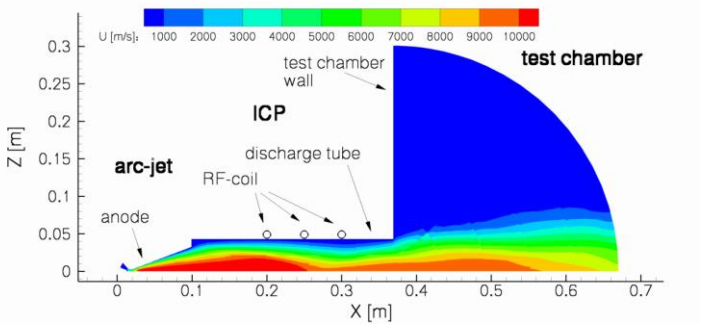

Figure 5: contour plot of the axial velocity (m/s) in TIHTUS

smaller values were used. These oscillations are assumed to be triggered and amplified by the mass flow controller. The conductivity limit creates an upper limit for the power that is coupled into the flow by the DC discharge according to $\vec{j}^2/\sigma$. The low degree of dissoziation and ionization at the available experiments with TIHTUS leads to no significant electrical conductivity. Hence, the induction in the second stage is very low and the computed power that is coupled into the plasma by the RF-discharge is too low, compared to the experiments.

The contour plot of the axial velocity component is shown in Figure 5 for the experimental case with $25\,\mathrm{kW}$ electrical input power in both the DC and the RF stage. The mass flow ratio is $\dot{m} = 300\,\mathrm{mg/s}$ of hydrogen. The point of maximum velocity is inside the ICP after the nozzle of the arc-jet. Figure 6 shows the radial plot of the measured and simulated axial velocity (m/s) 200 mm downstream the exit plane of the thruster. The maximum velocity at the centerline of the thruster compares well. Outside the core of the plasma plume the agreement gets worse. This is due to the low power that is coupled into the flow in the second stage. The second stage broadens the free stream plasma plume [26]. Figure 8 shows that the RF power coupled into the plasma is 4 orders of magnitude lower than the DC power. The induction takes place near the wall due to the skin effect. In the region near the discharge tube wall, the flow is in subsonic state, as can be seen from the local Mach number plot in Figure 7. This will increase the velocity of the flow. Only a very small amount of the RF power will couple into the supersonic area. In the supersonic case, the temperature will be increased by the inductive coupling.

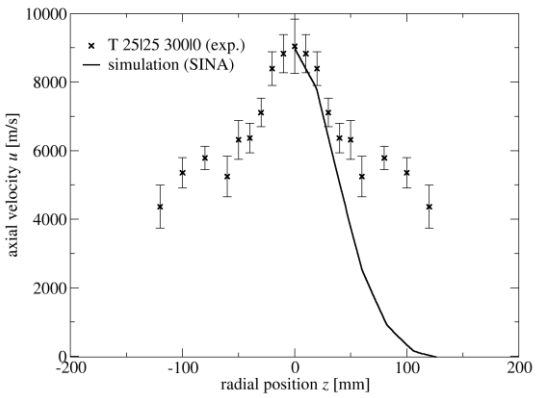

Figure 6: radial plot of the measured and simulated axial velocity (m/s) 200 mm downstream the exit plane of the thruster

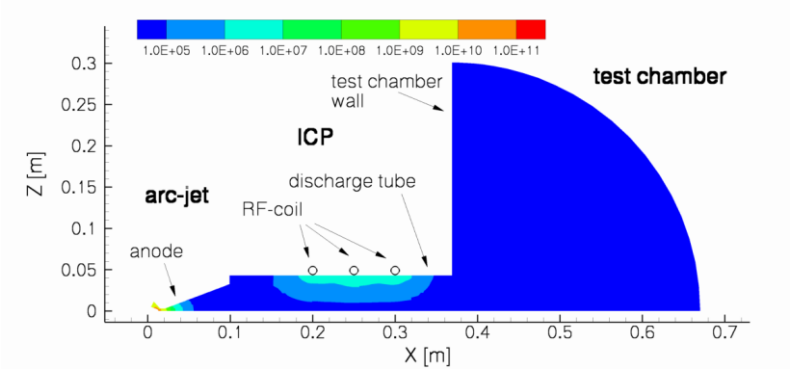

Figure 8: logarithmic contour plot of the ohmic heating source term (J/m^3) of both DC and RF solver in TIHTUS

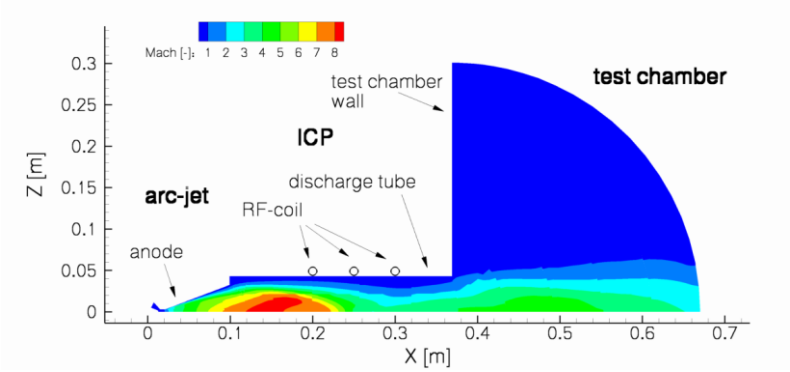

Figure 7: contour plot of the local Mach number in TIHTUS

V. Conclusion

The models for the simulation of DC-RF plasma thrusters with the Navier-Stokes Code SINA are described. This loosely coupled solver scheme includes the models for the simulation of the hypersonic viscous plasma flow in thermochemical non-equilibrium with both DC and RF discharge. With these models, a numerical simulation og the hybrid DC-RF thruster TIHTUS was performed for Hydrogen as working gas. The modified model of Scott was used with 6 Species and the three temperatures T, T_{vib}, T_e.

The axial velocity compares well with the experimental data only on the centerline of the thruster. The reason for this discrepancy is the fact, that less power is coupled into the plasma in the numerical simulation compared to the experiments. Due to the low DC and RF power the plasma is not ionized and hence the electrical conductivity is low. To prevent the solution from oscillations a lower limit for the electrical conductivity has to be applied which acts as an upper limit for the DC power in the simulation. Further improvements in the mass flow controller are

assumed to stabilize the simulations for a lower conductivity limit and hence allow the simulation to compute a higher coupling power. Nevertheless, the program runs stable with the above described models.

Acknowledgments

U. Bauder thanks Dr. Markus Fertig for valuable discussions about modeling and simulation of non-equilibrium plasma flows and Dr. Hannah Böhrk for the experimental data.

References

[1] Böhrk, H.: *Zur induktiven Nachheizung einer Überschallwasserstoff-strömung*, Dissertation, Institut für Raumfahrtsysteme, Universität Stuttgart, 2009.

[2] Auweter-Kurtz, M., Gölz, T. M., Habiger, H., Hammer, F., Kurtz, H., Riehle, M. and Sleziona, P. C.: High Power Hydrogen Arcjet Thrusters, *Journal of Propulsion and Power*, Vol. 14, No. 5, September 1998, p. 764–773.

[3] Bauder, U. und Auweter-Kurtz, M.: *Hydrogen Chemistry and Transport Coefficients for Simulation of the DC-RF thruster TIHTUS with the Loosely Coupled Navier-Stokes Code SINA*, International Electric Propulsion Conference 2011, Wiesbaden, Germany, 2011, IEPC-2011-084.

[4] Grau, T.: *Numerische Untersuchung von Plasmawindkanalströmungen zur Wiedereintrittssimulation* , Dissertation, Institut für Raumfahrt-systeme, Universität Stuttgart, 2000.

[5] Majid, A.: *Two phase flow solver for solid particles in hypersonic Martian entry flows*, Dissertation, Universität Stuttgart, Germany, 2011

[6] Gogel, T. H.: *Numerische Modellierung von Hochenthalpieströmungen mit Strahlungsverlusten* , Dissertation, Universität Stuttgart, Stuttgart, Germany, 1994.

[7] Gogel, T. H., Dupuis, M. und Messerschmid, E. W.: Radiation Transport Calculation in High Enthalpie Environments for Two–Dimensional Axisymetric Geometries, *Journal of Thermophysics and Heat Transfer* , Bd. 8, Nr. 4, 1994, p. 744–750.

[8] Smith, A. J., Wood, A., Dubois, J., Fertig, M. und Pfeiffer, B.: Plasma Radiation Database PARADE V2.2, *Techn. Ber. TR28/96 Issue 3* , Fluid Gravity Engineering Ltd, October 2006.

[9] Schmidt, A.: *Erzeugung eines Rechengitters für die Plasmaquelle RD5 und Berechnung einer Kaltgasströmung* , Studienarbeit, Universität Stuttgart, 1996, IRS-96-S-03.

[10] Program Development Corporation: *GridPro v5.5 User's Guide and Reference Manual*, 2012.

[11] Liou, M. S.: A Sequel to AUSM: AUSM+, *Journal of Computational Physics*, Bd. 129, Nr. 2, 1996, Seiten 364–382.

[12] Liou, M. S.: A sequel to AUSM, Part II: AUSM+ -up for all speeds, *Journal of Computational Physics*, Bd. 214, Nr. 1, 2006, Seiten 137–170.

[13] Rödiger, T.: *Analyse limitierter Extrapolationsverfahren zur Rekonstruktion von Hyperschallströmungen im thermochemischen Nichtgleichgewicht*, Diplomarbeit IRS 04-S-06 , Institut für Raumfahrtsysteme, Universität Stuttgart, Germany, 2004, .

[14] Fertig, M., Dohr, A. und Frühauf, H.-H.: Transport Coefficients for High Temperature Nonequilibrium Air Flows, *AIAA Journal of Thermophysics and Heat Transfer* , Bd. 15, Nr. 2, April 2001, Seiten 148–156.

[15] Chapman, S. and Cowling, T. G.: *The Mathematical Theory of Non-Uniform Gases*, Cambridge University Press, 3rd edition, 1970.

[16] Blazek, J.: Computational Fluid Dynamics: Principles and Applications, Elsevier, Burlington, Massachusetts, 2001.

[17] Park, C.: Convergence of Computation of Chemical Reacting Flows, *Progress in Astronautics and Aeronautics*, Vol. 103, 1986, p. 478–513.

[18] Scott, C. D.: Determining Electron Temperature and Density in a Hydrogen Microwave Plasma, *Journal of Thermophysics and Heat Transfer* , Vol. 10, Nr. 3, 1996, 426–435.

[19] Patch, R. W.: *Thermodynamic properties and theoretical rocket performance of hydrogen to 100, 000 K and 1. 01325 x 10 to the 8 th power N/sq m(Thermodynamic properties and theoretical rocket performance of hydrogen to 100, 000 K and 1.01325 x 10 to 8 th power N/sq m for chemical equilibrium in Debye-Huckel and ideal gas approximations)*, 1971.

[20] Höptner, J.: *Numerische Simulation der chemischen Reaktionen und der Transportkoeffizienten von Wasserstoff* , Diplomarbeit, Universität Stuttgart, 2010.

[21] Hirschfelder, J. O., Curtiss, C. F. und Bird, R. B.: *Molecular Theory of Gases and Liquids*, John Wiley & Sons, New York, 1954.

[22] Sleziona, P. C.: *Numerische Analyse der Strömungsvorgänge in magnetoplasmadynamischen Raumfahrtantrieben*, Dissertation, Universität Stuttgart, Germany

[23] Sleziona, P. C.: *Hochenthalpieströmungen für Raumfahrtanwendungen*, Shaker Verlag, Aachen, 1998.

[24] Mostaghimi, J. und Boulos, M. I.: *Two-dimensional electromagnetic field effects in induction plasma modelling*, Plasma Chemistry and Plasma Processing, Vol. 9, No. 1, 1989, p. 25–44.

[25] Bauder, U., Fertig, M., Böhrk, H., Herdrich, G., Petkow, D. und Auweter-Kurtz, M.: *Initiation of the Numerical Investigation of the Hybrid Plasma Thruster TIHTUS*, 30th IEPC , September 2007.

[26] Bauder, U.: *Numerische Simulation der induktiv beheizten Stufe des zweistufigen Plasmatriebwerks TIHTUS* , Diplomarbeit, Universität Stuttgart, January 2006, IRS-06-S-10.